Balkan Med J 2026;43:238-252

Ginkgetin Alleviates Doxorubicin-Induced Heart Failure by Regulating Mitochondrial Dysfunction Through the AMPK/Sirt1/NF-κB Signaling Pathway

Yanfu Wang[1#], Chong Wang[2#], Wei Li[1], Xinyu Ren[1], Yubo Peng[1], Yan Zhang[3]

[1]Department of Cardiovascular Medicine, Aviation General Hospital, Beijing, China
[2]Cardiac Center, Beijing Chest Hospital, Beijing, China
[3]Department of Rehabilitation Medicine, Beijing Chest Hospital, Beijing, China
[#]These authors contributed equally to this work

Background: Heart failure (HF) represents the terminal stage of many cardiovascular diseases. Doxorubicin (DOX) can induce HF through oxidative stress (OS), inflammation, and apoptosis. Ginkgetin (GK) has potential cardioprotective effects, but its underlying mechanisms remain unclear.

Aims: To investigate of GK against DOX-induced HF and explored its mechanisms, focusing on mitochondrial function and related signaling pathways.

Study Design: *In vivo* and *in vitro* experimental models.

Methods: HF was induced by DOX in mice and H9c2 cardiomyocytes. Cardiac function, myocardial injury, OS, inflammation, and apoptosis were assessed using echocardiography, biochemical assays, enzyme-linked immunosorbent assay, histopathology, immunofluorescence, and Western blot. Mitochondrial function was evaluated via transmission electron microscopy, RT-qPCR, and Seahorse analysis. Compound C was applied to verify the involvement of the adenosine monophosphate–activated protein kinase (AMPK)/Sirt1/nuclear factor-κB (NF-κB) pathway.

Results: GK markedly improved DOX-induced cardiac dysfunction and myocardial injury, reduced cardiac injury markers and inflammatory cytokines, and alleviated fibrosis, hypertrophy, apoptosis, and reactive oxygen species accumulation. GK restored superoxide dismutase activity, decreased malondialdehyde levels, increased glutathione and ATP, and preserved mitochondrial structure and respiratory function. GK upregulated AMPK and Sirt1, inhibited NF-κB activation, and regulated apoptosis-related proteins, whereas Compound C reversed these effects.

Conclusion: GK protects against DOX-induced HF by activating AMPK/Sirt1 and inhibiting NF-κB signaling, thereby mitigating OS, inflammation, apoptosis, and mitochondrial dysfunction.

INTRODUCTION

Heart failure (HF) is the end-stage manifestation of various cardiovascular disorders, characterized by impaired cardiac contractility, structural remodeling of the ventricles, and disrupted energy metabolism.[1,2] Despite significant advances in pharmacological therapies and device-based interventions, HF remains associated with high morbidity and mortality worldwide, representing a substantial public health burden.[3] HF progression involves multiple pathological factors, including oxidative stress (OS), mitochondrial dysfunction, genomic instability, apoptosis, inflammation, and calcium dysregulation.[4-7] Thus, elucidating the mechanisms underlying HF and identifying novel therapeutic strategies remain clinically essential.

Mitochondria, the central organelles for cardiomyocyte energy metabolism, play a critical role in HF pathogenesis.[8] Under physiological conditions, the mitochondrial electron transport chain generates ATP to sustain cardiac contractility.[9] However, during HF, imbalances in mitochondrial dynamics, excessive accumulation of reactive oxygen species (ROS), calcium dyshomeostasis, and impaired mitophagy collectively lead to energy deficiency and enhanced OS

Corresponding author: Yan Zhang, Department of Rehabilitation Medicine, Beijing Chest Hospital, Beijing, China

e-mail: n15853776810@hotmail.com

Received: November 12, 2025 **Accepted:** January 22, 2026 **Available Online Date:** 30.04.2026 • **DOI:** 10.4274/balkanmedj.galenos.2026.2025-11-113

Available at www.balkanmedicaljournal.org

ORCID iDs of the authors: Y.W. 0009-0007-5866-9531; C.W. 0009-0001-7202-404X; W.L. 0009-0000-3815-1646; X.R. 0009-0004-4968-5191; Y.P. 0000-0002-1447-1351; Y.Z. 0009-0000-5322-3206.

Cite this article as: Wang Y, Wang C, Li W, Ren X, Peng Y, Zhang Y. Ginkgetin Alleviates Doxorubicin-Induced Heart Failure by Regulating Mitochondrial Dysfunction Through the AMPK/Sirt1/NF-κB Signaling Pathway. Balkan Med J. 2026;43:238-252

in cardiomyocytes, ultimately promoting apoptosis and fibrosis.[10,11] Therefore, preserving or restoring mitochondrial function has emerged as a promising therapeutic strategy for HF management.

Adenosine monophosphate–activated protein kinase (AMPK) functions as a key regulator of cellular energy homeostasis, controlling mitochondrial biogenesis, lipid metabolism, and autophagy.[12] Activation of AMPK has been shown to reduce cardiac hypertrophy by inhibiting mammalian target of rapamycin signaling[13] and to enhance mitochondrial function through Sirt1/PGC-1α activation, thereby slowing HF progression.[14] Moreover, AMPK enhances Sirt1 activity, which regulates nuclear factor-κB (NF-κB) signaling to suppress inflammation and OS in cardiomyocytes.[15] Sirt1, an NAD(+)-dependent deacetylase, modulates energy metabolism and cell survival by deacetylating critical proteins such as p53 and NF-κB.[16,17] Overactivation of NF-κB exacerbates cardiac dysfunction by promoting excessive inflammation.[18] Collectively, targeting the AMPK/Sirt1/NF-κB pathway represents a potential strategy to correct mitochondrial dysfunction and mitigate HF progression.

Ginkgetin (GK), a bioactive biflavonoid derived from *Ginkgo biloba* leaves, exhibits multiple therapeutic effects, including antioxidative, anti-inflammatory, anticancer, antibacterial, and neuroprotective activities.[19,20] Emerging evidence highlights GK's potential in cardiovascular diseases. GK has been shown to mitigate myocardial injury caused by ischemia/reperfusion and improve cardiac function, primarily by reducing OS in cardiomyocytes.[21] Additionally, GK's anti-inflammatory properties suppress the release of inflammatory mediators, thereby alleviating inflammatory responses.[22] These features position GK as a promising natural compound for HF intervention.

This study aimed to investigate the cardioprotective effects of GK against doxorubicin (DOX)-induced HF, with a particular focus on its regulation of the AMPK/Sirt1/NF-κB pathway and consequent improvement of mitochondrial function. The findings provide both theoretical insights and experimental evidence for developing novel cardioprotective agents, offering potential strategies to enhance treatment safety in oncology patients.

MATERIALS AND METHODS

Animals

Male C57BL/6 mice (8 weeks old, 20–25 g) were purchased from SPF Biotechnology Co., Ltd. (Beijing, China; Animal Production License No.: SCXK [Jing] 2024-0001) and housed under controlled environmental conditions (temperature: 22 °C ±2 °C; relative humidity: 50% ±5%) with a 12-hour light/dark cycle (Animal Use License No.: SYXK [Jing] 2024-0010). After a one-week acclimatization period, mice were stratified by body weight to ensure no statistically significant differences in initial weights among groups. Subsequently, the mice were numbered and randomly assigned into six groups (n = 6 per group) using a computer-generated random number table: intraperitoneal injection of normal saline (control group); DOX group, receiving DOX (5 mg/kg, HY-15142, MCE) once weekly for four weeks to induce myocardial injury;[23] DOX + GK groups, receiving GK (25, 50, or 100 mg/kg, PHL83501, Sigma) once weekly for six weeks, starting one week before DOX administration; and the DOX + GK + Compound C group, receiving Compound C (20 mg/kg, HY-13418, MCE) prior to DOX treatment in combination with GK pretreatment.[24] Mice were monitored daily for general health throughout the experiment. At the study endpoint, mice were euthanized, and body weights were recorded. Hearts and tibias were collected to calculate the heart weight-to-tibia length ratio (HW/TL). All procedures, including drug administration and sample collection, were performed by researchers blinded to group allocation. Animal care and experimental procedures were conducted in accordance with regulations approved by the Aviation General Hospital Experimental Animal Ethics Committee (approval number: HK-X-2025-01, the date of the supplementary ethical annotation is: 13.01.2025).

Echocardiography

At the conclusion of the study, cardiac function was assessed using the VisualSonics Vevo 2100 ultrasound system in mice anesthetized with 2% isoflurane. Parameters measured included left ventricular ejection fraction (LVEF), left ventricular fractional shortening (LVFS), left ventricular end-systolic internal diameter (LVIDs), left ventricular end-diastolic internal diameter (LVIDd), and the mitral inflow E wave to A wave (E/A) ratio. All measurements were performed by a trained operator blinded to group allocation and treatment, and the average of three consecutive cardiac cycles was used for analysis.

Histopathology

Hematoxylin and eosin staining

Following the experimental protocol, cardiac tissues were harvested and fixed in 4% paraformaldehyde (PFA) for 24 hours. After standard dehydration and paraffin embedding, 4-μm sections were prepared. Tissue morphology was examined by hematoxylin and eosin (H&E) staining (C0105, Beyotime) and mounted with neutral resin (C0173, Beyotime), followed by microscopic observation using an Olympus BX53 microscope.

Masson trichrome staining

After deparaffinization and rehydration, myocardial sections were subjected to Masson trichrome staining (G1340, Solarbio) according to the manufacturer's protocol. The procedure involved sequential treatments with Weigert's hematoxylin, acidic ethanol differentiation solution, Ponceau fuchsin, phosphomolybdic acid, and aniline blue. Collagen fiber distribution was examined microscopically and quantitatively analyzed using ImageJ software to calculate the fibrosis area percentage.

Wheat germ agglutinin (WGA) staining

Paraffin-embedded sections were labeled with WGA-Alexa Fluor 488 (W11261, Invitrogen) to measure cardiomyocyte cross-sectional area. Sections were incubated at room temperature for 60 minutes, rinsed with PBS, and fluorescence images were captured using a Zeiss Axio Imager 2 microscope.

Dihydroethidium (DHE) staining

Superoxide anion levels were evaluated using dihydroethidium (DHE) staining (G4817, Solarbio). Cardiac tissues embedded in OCT compound (BL557A, Biosharp) were sectioned at 6-μm thickness, air-dried, and washed with PBS. Sections were then incubated with 5 μM DHE solution in the dark at 37 °C for 30 minutes in a humidified chamber. After additional PBS washes, fluorescence intensity was examined microscopically and quantified using ImageJ software.

Transmission electron microscopy (TEM)

Approximately 1 mm^3 fragments of cardiac tissue were immediately fixed in electron microscopy fixative (G1102, Servicebio) and maintained at 4 °C for 24 hours. Tissues were rinsed with PBS and postfixed in 1% osmium tetroxide (201030, Sigma) for 2 hours. After sequential alcohol dehydration and epoxy resin embedding, ultrathin sections were prepared and stained with uranyl acetate and lead citrate. Mitochondrial ultrastructure was examined and imaged using a Hitachi HT7800 transmission electron microscope.

Real-time quantitative polymerase chain reaction

Total ribonucleic acid (RNA) was extracted from myocardial tissue using TRIzol reagent (15596026, Invitrogen), and RNA concentration and purity were assessed with a NanoDrop 2000 spectrophotometer (Thermo). Complementary DNA was synthesized using a commercial reverse transcription kit (R323-01, Vazyme). Quantitative real-time polymerase chain reaction (PCR) was performed with SYBR Green PCR Master Mix (11184ES08, Yeasen) on a LightCycler 480 system (Roche), using the primers listed in Table 1. Relative gene expression was calculated using the 2^−ΔΔCt method, with GAPDH as the endogenous control. The experiment included six independent biological replicates (n = 6), with each replicate measured in triplicate as technical replicates.

Cell culture and treatment

The H9c2 rat cardiomyocyte line (ZKCC62184, ZKCC) was cultured in DMEM medium (ZKCC809466, ZKCC) supplemented with 10% fetal bovine serum and 1% antibiotic-antimycotic solution at 37 °C in a 5% CO_2 atmosphere (Thermo 150i/240i). Experimental groups included: (i) untreated controls, (ii) DOX-challenged cells, and (iii) DOX-treated cells with GK preconditioning (5, 10, or 20 μM for 24 hours). To further explore GK's mechanism, an additional group received combined GK and Compound C (20 μM each) prior to DOX exposure.[25]

Cell viability assays

Cell counting kit-8 (CCK-8) assay

Cell viability was assessed using the cell counting kit-8 (CCK-8) assay (A311-01, Vazyme). H9c2 cells were seeded at 2×10^3 cells/well in 96-well plates and cultured for 24 hours. Cells were treated with various GK concentrations (0, 2, 5, 10, 20, 40, or 80 μM) for 24 or 48 hours. After adding 10 μL of CCK-8 reagent, cells were incubated at 37 °C for 2 hours in the dark, and absorbance was measured at 450 nm. For DOX experiments, cells were pretreated with GK before exposure to 5 μM DOX for 24 hours, after which viability was evaluated.

Calcein AM/ethidium homodimer-1 (EthD-1) double staining

Cardiomyocyte viability was further assessed using a dual-fluorescence assay (Calcein AM/EthD-1, IKA10403, Solarbio). After overnight culture in 6-well plates, cells were washed with PBS and incubated with the working solution for 20 minutes at room temperature. Following additional PBS washes, nuclei were counterstained with Hoechst 33342 (H3570, Invitrogen). Viable cells were visualized as green cytoplasmic fluorescence, while non-viable cells exhibited red nuclear fluorescence, and the percentages of live and dead cells were quantified.

In vitro ROS detection

Intracellular ROS levels were measured using the DCFH-DA probe (C2938, Invitrogen). H9c2 cells were seeded in 96-well plates, treated as described, and incubated with 10 μM DCFH-DA at 37 °C in the dark for 30 minutes. Cells were washed three times with PBS, observed under a fluorescence microscope, and fluorescence intensity was quantified using ImageJ software. Fluorescence intensity was used as an indicator of intracellular ROS levels. To evaluate mitochondrial OS, MitoTracker-RFP (C10601, Invitrogen) and DCFH-DA were applied for colocalization analysis. Cardiomyocytes on coverslips were first stained with 30 nM MitoTracker-RFP for 30 minutes at room temperature, followed by DCFH-DA treatment. Fluorescence images were captured and quantitatively analyzed.

Mitochondrial membrane potential (MMP) detection

Mitochondrial membrane potential (MMP) was assessed using the JC-1 fluorescent probe (T3168, Invitrogen). After experimental treatments, cells were washed with PBS and incubated with JC-1 working solution (10 μg/mL) for 30 minutes at 37 °C in the dark. Following additional PBS washes, JC-1 fluorescence patterns were observed under a microscope. In polarized mitochondria, JC-1 forms

TABLE 1. RT-qPCR Primer Sequences.

Gene	Accession	Forward primer (5'→3')	Reverse primer (5'→3')
MDH	NM_008617.2	GACCTGTTCAACACCAACGC	GGATGGTGGAGTTCACTGGG
NNT	NM_001308506.1	CAGCTCTGATTCCAGGTGGT	CCACCGTAGAGAGCAGCTAAA
PDH	NM_008810.3	CTGCCTATTGCAGGTCTGGT	TTCTTCTCGAGTGCGGTAGC
GAPDH	NM_001411842.1	TGACCTCAACTACATGGTCTACA	CTTCCCATTCTCGGCCTTG

red fluorescent J-aggregates, whereas depolarized mitochondria display green monomers. MMP changes were quantified as the green-to-red fluorescence intensity ratio, with higher ratios indicating mitochondrial depolarization.

Mitochondrial respiratory function

Mitochondrial bioenergetics were analyzed using the Seahorse XFp system (Seahorse Bioscience). H9c2 cells were seeded at 4×10^4 cells/well in 96-well plates and incubated in XF base medium (103575-100, Agilent; pH 7.4) supplemented with 1 mM pyruvate, 2 mM glutamine, and 10 mM glucose. Sequential injections of oligomycin, FCCP, and rotenone/antimycin A were performed to measure basal respiration, maximal respiration, and spare respiratory capacity.

Biochemical assays

At the conclusion of *in vivo* experiments, blood was collected from the retro-orbital plexus and allowed to coagulate. Serum was obtained by centrifugation at 3,000 rpm for 10 minutes and stored at –80 °C. Myocardial tissues were dissected, rinsed with ice-cold physiological saline, and either cryopreserved in liquid nitrogen or processed immediately. *In vitro*, treated H9c2 cells were lysed by ultrasonic disruption (SCIENTZ-IID) and centrifuged at 8,000 × g for 10 minutes at 4 °C, with supernatants kept on ice for subsequent biochemical assays. Each treatment condition included a minimum of six technical replicate wells per plate. Data acquisition and analysis were performed by operators blinded to group allocation to minimize bias.

Lactate dehydrogenase (LDH) assay

Lactate dehydrogenase (LDH) activity in mouse serum and cardiomyocytes was measured using an LDH assay kit (BC0680, Solarbio) by visible spectrophotometry. The spectrophotometer (DU800, Beckman) was preheated for 60 minutes to ensure stability, and absorbance was measured at 450 nm. The assay was conducted according to the manufacturer's instructions. A standard curve was generated, and serum samples (10 µL) were incubated with the working reagent. After reaction termination, optical density at 450 nm (OD450) was immediately recorded using a Synergy H1 microplate reader (BioTek). LDH activity (U/L) was calculated based on the regression equation of the standard curve.

OS index assays

Heart tissues were homogenized in ice-cold extraction buffer at a 1:10 tissue-to-buffer ratio, followed by centrifugation at 12,000 × g for 10 minutes at 4 °C. The resultant heart homogenates and cardiomyocyte supernatants were used to determine OS indices. Superoxide dismutase (SOD, BC5165, Solarbio), glutathione (GSH, BC1175, Solarbio), and malondialdehyde (MDA, BC6415, Solarbio) levels were measured using commercial assay kits according to absorbance at 450, 412, and 532 nm, respectively.

ATP content assay

ATP levels were quantified using a commercial kit (BC0300, Solarbio). Tissue homogenates were chloroform-extracted and centrifuged at 10,000 × g for 3 minutes at 4 °C. Supernatant absorbance at 340 nm was measured, and ATP content was calculated from standard curves.

Enzyme-linked immunosorbent assay (ELISA)

Serum and cellular levels of myocardial injury markers [B-type natriuretic peptide (BNP, MBS163925), creatine kinase-MB (CK-MB, MBS265110), and cardiac troponin T (cTnT, MBS3805826)] and inflammatory factors [NO (MBS2608310), cyclooxygenase-2 (COX-2; MBS3807482; MBS725633), tumor necrosis factor-alpha (TNF-α) (MBS494101; MBS9424865), and interleukin-6 (IL-6) (MBS286952; MBS2515034)] were measured using MyBioSource (California, USA) enzyme-linked immunosorbent assay (ELISA) kits according to the manufacturer's protocols. Absorbance was read at 450 nm, and analyte concentrations were determined using calibration curves.

Terminal deoxynucleotidyl transferase dUTP nick end labeling (TUNEL) staining

Myocardial paraffin sections were dewaxed, hydrated, and digested with proteinase K (20 µg/mL, 37 °C, 15 minutes). H9c2 cells on coverslips were fixed with 4% PFA for 15 minutes at room temperature and washed with PBS. Samples were permeabilized with 0.1% Triton X-100 for 10 minutes prior to terminal deoxynucleotidyl transferase dUTP nick end labeling (TUNEL) staining (C10617, Invitrogen) at 37 °C for 1 hour. After DAPI counterstaining for 5 minutes and mounting with P0126 (Beyotime), apoptotic cells were quantified in five randomly selected fields under a fluorescence microscope.

Immunofluorescence

Cardiomyocytes were fixed in 4% PFA, permeabilized with 0.2% Triton X-100, and blocked with 5% BSA. Paraffin sections were dewaxed, hydrated, and subjected to antigen retrieval and blocking. Primary antibodies, anti-γ-H2AX (ab81299, 1:250, Abcam) and anti-p-NF-κB p65 (#8242, 1:400, CST), were applied overnight at 4 °C. Following PBS washes, samples were incubated with fluorescent secondary antibodies (B40943/B40944, Invitrogen) for 1 hour at room temperature in the dark, counterstained with DAPI, and visualized by fluorescence microscopy.

Western blot

Protein extracts from cardiac tissues or H9c2 cells were prepared using RIPA buffer (R0010, Solarbio), and concentrations were determined by BCA assay (PC0040, Solarbio). Proteins were separated by SDS-PAGE and transferred onto PVDF membranes. Membranes were blocked with 5% milk for 1 hour at room temperature and incubated overnight at 4 °C with primary antibodies: Bax (ab32503, Abcam), Bcl-2 (ab194583, 1:500, Abcam), cleaved-caspase 3 (#9661, CST), caspase 3 (#9662, CST), AMPK (ab32047, Abcam), p-AMPK (ab133448, Abcam), Sirt1 (ab189494, Abcam), NF-κB p65 (#8242, CST), p-NF-κB p65 (#3033, CST), and GAPDH (#2118, CST) at 1:1000 dilution. After TBST washing, membranes were incubated with HRP-conjugated secondary antibodies (1:5000, #7074, CST) for 1 hour at room temperature. Protein signals were detected using enhanced chemiluminescence (P0018, Beyotime) on a Tanon 5200 imaging system. Band intensities were quantified using ImageJ and normalized to GAPDH. Each membrane contained samples from all experimental groups, and the operator remained blinded to group allocation throughout the analysis.

Statistical analysis

All data are presented as mean ± standard deviation. No a priori sample size calculation was performed; instead, the sample size was determined with reference to previously published literature[26,27] and practical feasibility considerations. Sensitivity analysis indicated that, under $\alpha = 0.05$ and power = 0.8, this sample size provided sufficient power to detect large effect sizes, and the results are therefore interpreted primarily as exploratory evidence for large effects. Normality was assessed using the Shapiro–Wilk test, and homogeneity of variances was evaluated with Levene's test. Multiple group comparisons were conducted using one-way analysis of variance followed by Bonferroni post-hoc tests. A p value of less than 0.05 was considered statistically significant. All data processing and analyses were performed by researchers blinded to group allocation.

RESULTS

GK ameliorates DOX-induced cardiac dysfunction in mice

A mouse model of myocardial injury induced by DOX was established to systematically investigate the cardioprotective mechanisms of GK. Experimental data showed that DOX exposure caused a significant reduction in body weight (Figure 1a), which was notably reversed by GK, particularly at the higher dose of 100 mg/kg. Additionally, DOX-treated mice exhibited an increased HW/TL ratio (Figure 1b), indicative of cardiac hypertrophy or fluid retention. This pathological change was dose-dependently alleviated by GK, supporting its potential role in preventing DOX-induced cardiac structural abnormalities.

Cardiac functional assessment revealed that DOX administration significantly impaired cardiac performance compared with controls, as evidenced by reduced LVEF, fractional shortening (LVFS), and E/A ratio, along with elevated left ventricular end-systolic and end-diastolic internal diameters (LVIDs and LVIDd). GK treatment dose-dependently restored these parameters (Figure 1c-g), demonstrating its efficacy in counteracting DOX-induced cardiac dysfunction, with the 100 mg/kg dose achieving near-normalization.

Serum analyses further indicated that GK attenuated DOX-induced elevations of myocardial injury biomarkers, including LDH, CK-MB, and cTnT, as well as HF marker BNP (Figure 1h-k). These findings suggest that GK may protect cardiomyocytes from DOX cytotoxicity by preserving membrane integrity and supporting energy metabolism.

Histopathological evaluation revealed that DOX treatment induced marked myocardial abnormalities, including disordered myocardial fiber arrangement, interstitial fibrosis, and cardiomyocyte hypertrophy, whereas GK treatment significantly improved these features (Figure 1l-n). Specifically, H&E staining showed that GK reduced myocardial cell degeneration, necrosis, and inflammatory infiltration; Masson trichrome staining demonstrated inhibition

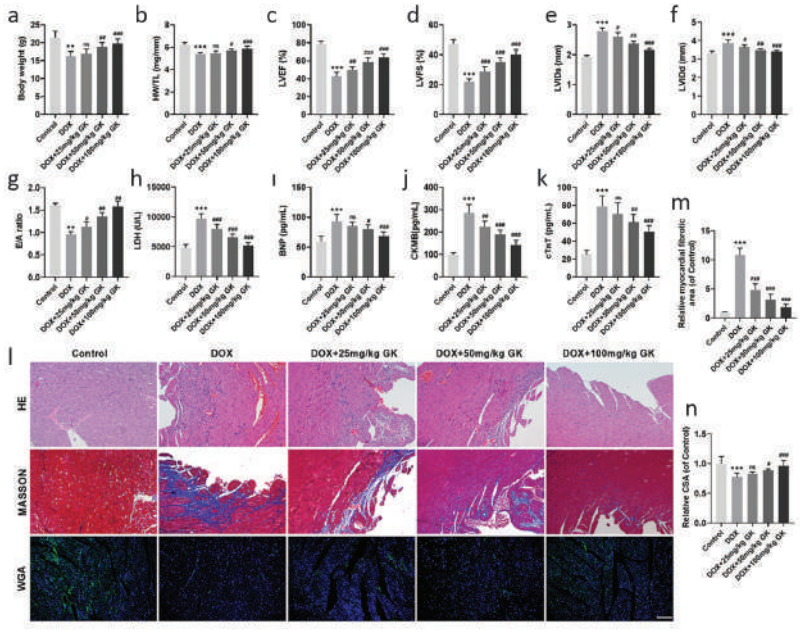

FIG. 1. GK ameliorates DOX-induced cardiac dysfunction in mice. (a) Mice were randomly assigned to five groups: Control, DOX model, and DOX + GK (25, 50, 100 mg/kg). Body weight changes were monitored to evaluate general health status. (b) HW/TL ratio was determined to assess DOX-induced cardiac edema and GK's therapeutic effect. (c-g) Cardiac function (LVEF, LVFS, LVIDs, LVIDd, E/A) was analyzed to evaluate GK's improvement on DOX-induced dysfunction. (h-k) Serum markers (LDH, CK-MB, cTnT, BNP) were measured to investigate GK's cardioprotective effects against DOX injury. (l-n) Myocardial pathology was examined using HE, Masson, and WGA staining to assess structural improvements by GK treatment. Scale bar 100 μm. n = 6. $^{**}p < 0.01$, $^{***}p < 0.001$ vs. Control; ns $p > 0.05$, $^{\#}p < 0.05$, $^{\#\#}p < 0.01$, $^{\#\#\#}p < 0.001$ vs. DOX. LVEF, left ventricular ejection fraction; LVFS, left ventricular fractional shortening; LVIDs, left ventricular end-systolic internal diameter; LVIDd, left ventricular end-diastolic internal diameter; E/A, E wave to A wave; GK, ginkgetin; DOX, doxorubicin; LDH, lactate dehydrogenase; CK-MB, creatine kinase-MB; cTnT, cardiac Troponin T; BNP, B-type natriuretic peptide; HW/TL, heart weight-to-tibia length ratio; WGA, wheat germ agglutinin.

of interstitial fibrosis; and WGA staining indicated alleviation of cardiomyocyte hypertrophy. Collectively, these data suggest that GK protects against DOX-induced cardiotoxicity (DIC) by improving cardiac function while mitigating myocardial injury and pathological remodeling.

GK attenuates DOX-induced myocardial inflammation, OS, and apoptosis in mice

The effects of GK on DOX-induced cardiac inflammation were further examined. ELISA results showed that DOX treatment markedly increased serum levels of inflammatory markers, including NO, COX-2, TNF-α, and IL-6 (Figure 2a-d). GK dose-dependently attenuated these inflammatory responses, with the most pronounced effects observed at 100 mg/kg, indicating significant anti-inflammatory activity against DIC. Assessment of OS demonstrated significantly elevated ROS generation in myocardial tissues of DOX-treated mice, as evidenced by intensified DHE fluorescence signals (Figure 2e, f). GK intervention effectively reduced this oxidative burden in a dose-dependent manner. Biochemical analyses further revealed that DOX exposure substantially decreased myocardial antioxidant defenses (SOD and GSH) while increasing lipid peroxidation (MDA) (Figure 2g-i). These perturbations were significantly reversed by GK administration, confirming its therapeutic potential against DOX-induced oxidative myocardial injury.

Quantitative analysis of TUNEL-stained myocardial sections indicated a significant increase in apoptotic cell death following DOX treatment compared with controls (Figure 2j, k). Western blot analyses revealed notable changes in key apoptotic regulators, including upregulated Bax expression, downregulated Bcl-2 levels, and increased caspase-3 activation, as indicated by elevated cleaved-caspase 3/caspase 3 ratios (Figure 2l, m). GK treatment dose-dependently mitigated these apoptotic alterations, demonstrating its regulatory effects on apoptotic signaling pathways. Taken together, these findings indicate that GK exerts comprehensive cardioprotective effects by suppressing inflammatory cytokine production, enhancing endogenous antioxidant defenses, and modulating apoptotic machinery through regulation of Bcl-2 family proteins and caspase-3 activity.

GK improves DOX-induced mitochondrial dysfunction in mouse Myocardium

Building upon these findings, the potential of GK to ameliorate DOX-induced mitochondrial impairment was investigated. TEM revealed that mitochondria in control hearts exhibited normal morphology, with oval or elongated shapes, intact ultrastructure, densely packed and well-organized cristae, and regular distribution between myofibrils. In contrast, mitochondria in the DOX group displayed pronounced structural abnormalities, including reduced mitochondrial number, condensed and shrunken mitochondria, aggregation of morphologically aberrant mitochondria, and disrupted cristae architecture. GK treatment markedly improved both mitochondrial number and ultrastructure, indicating effective preservation of mitochondrial integrity (Figure 3a).

The interplay between DNA damage and mitochondrial dysfunction forms a self-perpetuating pathological cycle, whereby compromised DNA integrity disrupts mitochondrial homeostasis, while mitochondrial-derived OS exacerbates genomic instability.[28] Immunofluorescence analysis revealed that DOX administration significantly increased γ-H2AX foci formation, a sensitive marker of DNA double-strand breaks. Importantly, GK dose-dependently attenuated γ-H2AX immunoreactivity (Figure 3b, c), demonstrating

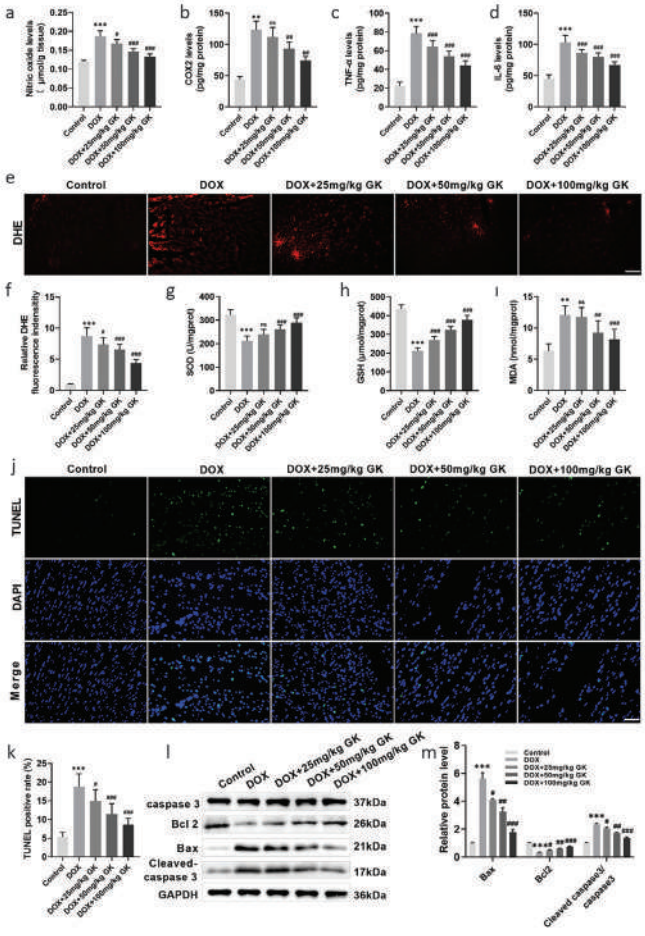

FIG. 2. GK attenuates dox-induced myocardial inflammation, OS, and apoptosis in mice. (a-d) Serum inflammatory mediators (NO, COX-2, TNF-α, IL-6) were quantified by ELISA to examine GK's modulation of DOX-triggered systemic inflammation. (e, f) Myocardial ROS accumulation was visualized through DHE staining and quantified by fluorescence intensity analysis. Scale bar 100 μm. (g-i) The antioxidant defense system (SOD, GSH) and lipid peroxidation (MDA) in cardiac tissue were evaluated using biochemical assays to determine GK's protection against DOX-mediated oxidative stress (OS). (j, k) Apoptotic cardiomyocytes were identified via TUNEL assay following DOX exposure and GK treatment. Scale bar 50 μm. (l, m) Protein immunoblotting revealed GK's regulation of apoptosis markers (Bax, Bcl-2, Cleaved-caspase 3/caspase 3) in DOX-challenged myocardium. n = 6. $^{**}p < 0.01$, $^{***}p < 0.001$ vs. Control; ns $p > 0.05$, $^{\#}p < 0.05$, $^{\#\#}p < 0.01$, $^{\#\#\#}p < 0.001$ vs. DOX. DOX, doxorubicin; GK, ginkgetin; ROS, reactive oxygen species; ELISA, enzyme-linked immunosorbent assay; COX-2, cyclooxygenase-2; DHE, dihydroethidium.

its protective effect against DOX-induced genotoxic stress in cardiomyocytes.

Mitochondrial dysfunction also impairs oxidative phosphorylation, reducing ATP synthesis and disrupting energy metabolism.[29,30] Biochemical analyses showed that DOX treatment depleted myocardial ATP levels and downregulated transcription of key mitochondrial enzymes, including PDH, MDH, and NNT. GK treatment restored the expression of these enzymes and increased ATP production in a dose-dependent manner, thereby normalizing myocardial energy metabolism (Figure 3d-g). Collectively, these results demonstrate that GK ameliorates DOX-induced mitochondrial dysfunction through multiple complementary mechanisms, including preservation of mitochondrial ultrastructure, attenuation of genotoxic stress, restoration of metabolic enzyme expression, and enhancement of bioenergetic capacity.

GK alleviates DOX-induced HF in mice by improving mitochondrial dysfunction via the AMPK/Sirt1/NF-κB signaling pathway

The cardioprotective mechanism of GK was further investigated through modulation of the AMPK/Sirt1/NF-κB signaling axis *in vivo*. Western blot analysis revealed that DOX administration markedly suppressed cardiac Sirt1 expression and AMPK activation (p-AMPK) while simultaneously enhancing NF-κB p65 phosphorylation (Figure 4a, b). Immunofluorescence analysis confirmed that DOX significantly increased p-NF-κB p65 expression in mouse myocardium (Figure 4c, d). In contrast, GK treatment significantly upregulated Sirt1 protein expression and AMPK phosphorylation and markedly downregulated p-NF-κB p65 expression, indicating effective activation of the AMPK/Sirt1 pathway and inhibition of NF-κB signaling. Notably, co-administration of the AMPK inhibitor Compound C attenuated these protective effects, suggesting that the cardioprotective action of GK predominantly depends on regulation of the AMPK/Sirt1/NF-κB axis.

Mitochondrial functional assays showed that DOX-treated myocardial tissue exhibited increased γ-H2AX expression, reduced ATP production, and downregulated mRNA levels of mitochondrial metabolic enzymes (MDH, NNT, and PDH) (Figure 4e-j), indicating DOX-induced mitochondrial dysfunction as a key mechanism of myocardial injury. GK treatment significantly ameliorated these mitochondrial deficits, and these improvements were partially reversed by Compound C. These findings demonstrate that GK mitigates DOX-induced HF in mice by improving mitochondrial function through modulation of the AMPK/Sirt1/NF-κB signaling pathway.

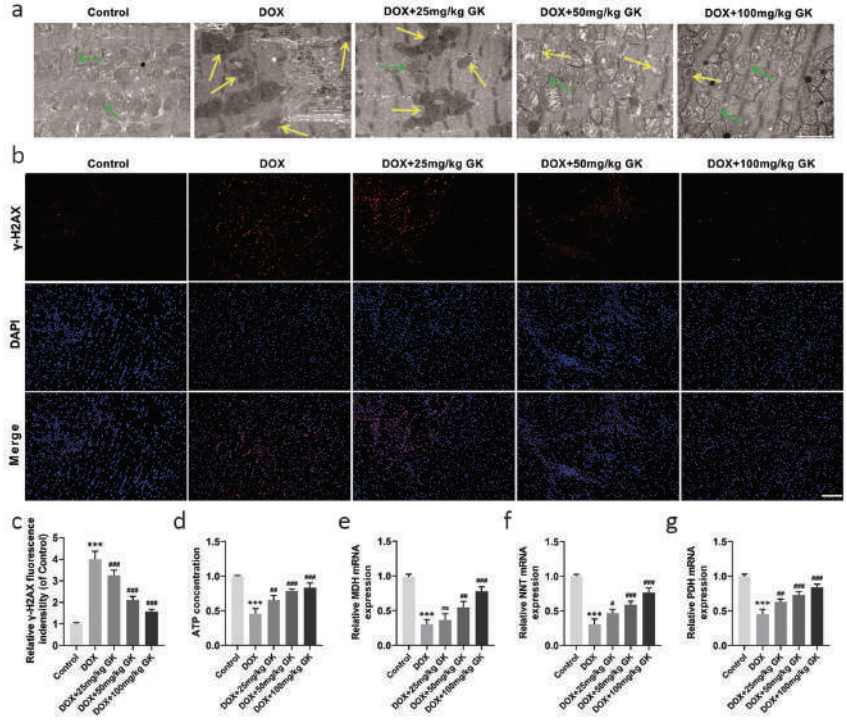

FIG. 3. GK improves DOX-induced mitochondrial dysfunction in mouse myocardium. (a) Mitochondrial ultrastructure in cardiomyocytes was examined using transmission electron microscopy. Green indicates mitochondria with normal structure, while yellow indicates mitochondria with structural abnormalities, including condensation and cristae fragmentation. Scale bar 2 μm. (b, c) γ-H2AX expression, as a DNA damage indicator, was visualized and quantified in myocardial sections through immunofluorescence analysis. Scale bar 100 μm. (d) Myocardial ATP levels were determined to evaluate mitochondrial metabolic function. (e-g) Transcript levels of key mitochondrial metabolic genes (MDH, NNT, PDH) were assessed by quantitative real-time PCR. n = 6. $^{***}p < 0.001$ vs. Control; ns $p > 0.05$, $^{\#}p < 0.05$, $^{\#\#}p < 0.01$, $^{\#\#\#}p < 0.001$ vs. DOX. DOX, doxorubicin; GK, ginkgetin; PCR, polymerase chain reaction.

GK improves DOX-induced cardiomyocyte viability impairment

To examine GK's potential in protecting cardiomyocytes *in vitro*, H9c2 cells were exposed to varying concentrations of GK (0, 2, 5, 10, 20, 40, 80 μM) for 24 or 48 h, and cell viability was assessed using the CCK-8 assay. No significant cytotoxicity was observed at any tested concentration (Figure 5a). In contrast, DOX treatment alone substantially reduced H9c2 cell viability. GK exhibited a dose-dependent protective effect at 5, 10, and 20 μM, significantly improving cell survival (Figure 5b), and these concentrations were selected for subsequent experiments.

The LDH release assay further confirmed GK's protective effect. DOX treatment significantly increased LDH release from cardiomyocytes, whereas GK dose-dependently reduced LDH release (Figure 5c), indicating attenuation of DOX-induced membrane damage. Fluorescence imaging revealed elevated cardiomyocyte mortality following DOX exposure, characterized by increased red fluorescence of non-viable cells and reduced green fluorescence of viable cells (Figure 5d-f). GK treatment restored normal cellular morphology and viability, resulting in higher survival rates and decreased cell death, consistent with the *in vivo* cardioprotective effects of GK.

GK attenuates DOX-induced cardiomyocyte inflammation, OS, and apoptosis

The cardioprotective mechanisms of GK were further examined in DOX-treated H9c2 cardiomyocytes. ELISA analyses showed that DOX significantly increased secretion of pro-inflammatory mediators, including TNF-α, IL-6, and COX-2, which were dose-dependently attenuated by GK, confirming its anti-inflammatory properties (Figure 6a-c). Intracellular OS, assessed using DCFH-DA fluorescence, was markedly elevated by DOX treatment, accompanied by decreased SOD activity and increased MDA content. GK treatment effectively reversed these alterations, reducing ROS accumulation, restoring SOD activity, and decreasing MDA levels (Figure 6d-g), demonstrating robust protection against OS *in vitro*.

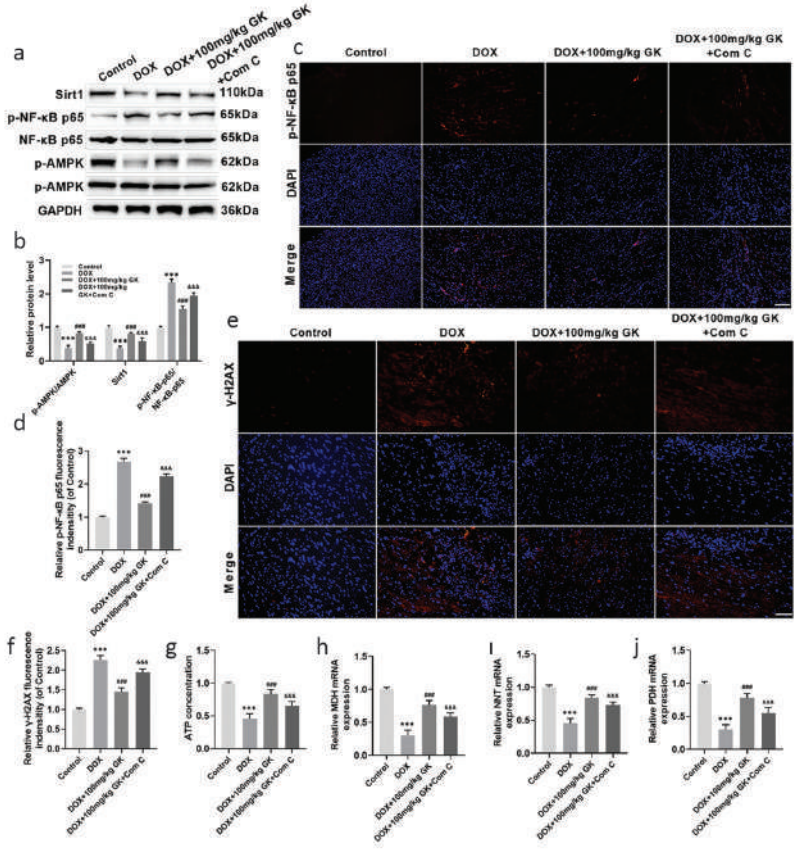

FIG. 4. GK alleviates DOX-induced HF in mice by improving mitochondrial dysfunction through the AMPK/Sirt1/NF-κB signaling pathway. (a, b) To elucidate GK's cardioprotective mechanisms against DOX-induced HF, four treatment groups were analyzed: Control, DOX, DOX + GK, and DOX + GK + Com C. Protein expression profiles of AMPK/Sirt1/NF-κB pathway components (AMPK, p-AMPK, Sirt1, NF-κB p65, p-NF-κB p65) were examined in cardiac tissues by immunoblotting. (c, d) Nuclear translocation of p-NF-κB p65 was visualized through immunofluorescence to determine NF-κB pathway activation status. Scale bar 50 μm. (e, f) Mitochondrial DNA damage was evaluated by quantifying γ-H2AX foci formation using immunofluorescence microscopy. Scale bar 50 μm. (g) Myocardial bioenergetic status was determined by measuring ATP production across experimental groups. (h-j) Transcript abundance of mitochondrial metabolic regulators (MDH, NNT, PDH) was quantified using RT-qPCR analysis. n = 6. $^{***}p < 0.001$ vs. Control; $^{\#\#\#}p < 0.001$ vs. DOX; $^{\&\&\&}p < 0.001$ vs. DOX + 100 mg/kg GK. DOX, doxorubicin; GK, ginkgetin; HF, heart failure; NF-κB, nuclear factor-κB; AMPK, adenosine monophosphate–activated protein kinase.

Apoptotic analysis using TUNEL staining and immunoblotting revealed that DOX markedly increased cardiomyocyte apoptosis, characterized by upregulation of pro-apoptotic mediators (Bax and cleaved caspase-3) and downregulation of the anti-apoptotic protein Bcl-2 (Figure 6h-k). GK treatment significantly reduced apoptosis and normalized the expression of apoptosis-related proteins, effectively inhibiting caspase-3 activation. Together with the *in vivo* results, these findings indicate that GK prevents DOX-mediated cardiomyocyte injury through coordinated modulation of inflammation, OS, and apoptosis.

GK ameliorates DOX-induced mitochondrial dysfunction in cardiomyocytes

GK's effects on DOX-induced mitochondrial impairment in cardiomyocytes were comprehensively assessed through multiple experimental approaches. MMP, a critical indicator of respiratory chain function and cellular energy homeostasis,[31] was evaluated using JC-1 staining. DOX treatment significantly reduced MMP, as indicated by an increased green/red fluorescence ratio, whereas GK dose-dependently restored MMP stability (Figure 7a, b). DOX also elevated mitochondrial ROS levels in cardiomyocytes, which were markedly reduced by GK pretreatment (Figure 7c, d). Immunofluorescence analysis showed that DOX significantly increased γ-H2AX fluorescence intensity, reflecting mitochondrial DNA damage, whereas GK dose-dependently decreased γ-H2AX signals, demonstrating protection against genotoxic stress (Figure 7e, f).

Mitochondrial function analyses revealed that DOX decreased ATP production (Figure 7g) and impaired respiratory activity, as shown by reduced basal and maximal oxygen consumption rates and diminished spare respiratory capacity in Seahorse XFp assays (Figure 7h-k). GK treatment significantly improved these parameters, enhancing ATP synthesis and restoring mitochondrial respiratory function. Collectively, these findings confirm that GK exerts broad mitochondrial protective effects, including stabilization of membrane potential, reduction of OS, prevention of DNA damage, and optimization of respiratory chain function in cardiomyocytes.

GK Alleviates DOX-induced cardiomyocyte injury by improving mitochondrial dysfunction via the AMPK/Sirt1/NF-κB signaling pathway

In vitro protein expression profiling confirmed the mechanistic pathway modulation observed *in vivo*. DOX disrupted the AMPK/Sirt1/NF-κB signaling axis, while GK treatment significantly reversed these effects by upregulating p-AMPK and Sirt1 and suppressing p-NF-κB p65 expression (Figure 8a, b). Pharmacological inhibition with Compound C largely abolished GK's regulatory effects, indicating that its cardioprotective actions are primarily mediated via the AMPK/Sirt1/NF-κB pathway.

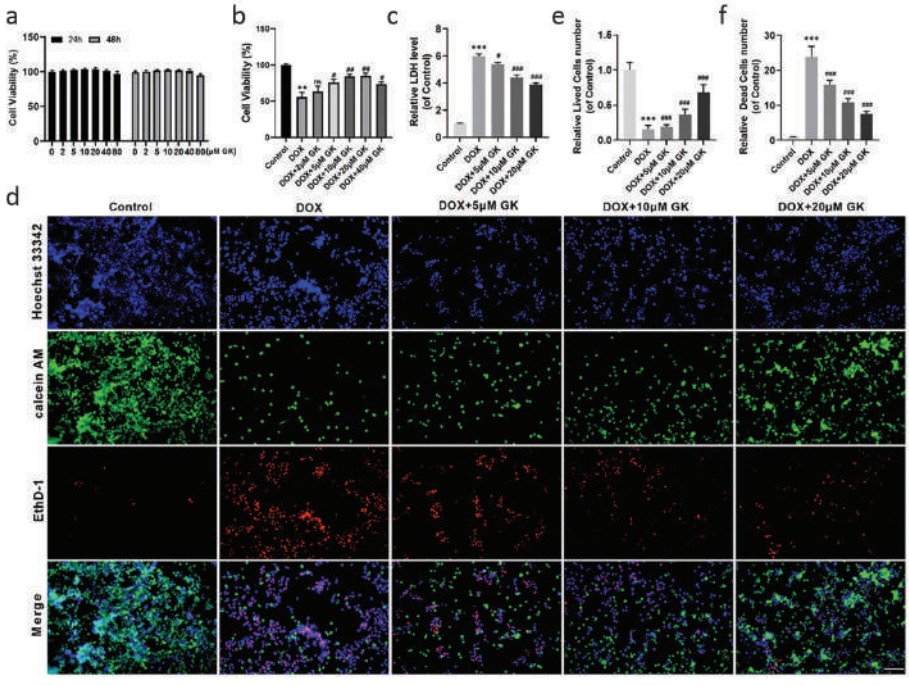

FIG. 5. GK improves DOX-induced cardiomyocyte viability impairment. (a, b) The cytoprotective potential of GK (0/2/5/10/20/40/80 μM) against DOX-induced injury was evaluated in H9c2 cells using CCK-8 viability assays. Three treatment conditions (control, DOX-only, and DOX + GK) were established, with subsequent studies focusing on the 5, 10, and 20 μM GK range demonstrating significant protective effects. (c) The degree of cardiomyocyte injury was determined through LDH release measurements. (d-f) A dual-viability staining approach was employed, combining Hoechst 33342 for nuclear visualization (blue), Calcein AM for metabolically active cells (green), and EthD-1 for membrane-compromised cells (red). Quantitative analysis was conducted for the fluorescence intensity of live cells and dead cells. Scale bar 100 μm. n = 6. $^{**}p < 0.01$, $^{***}p < 0.001$ vs. Control; ns $p > 0.05$, $^{\#}p < 0.05$, $^{\#\#}p < 0.01$, $^{\#\#\#}p < 0.001$ vs. DOX. DOX, doxorubicin; GK, ginkgetin; CCK-8, Cell counting kit-8; LDH, lactate dehydrogenase.

Functional analyses corroborated these findings. JC-1 staining demonstrated that GK prevented DOX-induced MMP dissipation, an effect substantially attenuated by co-treatment with Compound C (Figure 8c, d). Similarly, GK reduced mitochondrial ROS levels in an AMPK-dependent manner (Figure 8e, f). Mechanistic studies further revealed that the AMPK/Sirt1/NF-κB axis mediates GK's protective effects, including mitigation of DNA damage, enhancement of ATP synthesis, and restoration of mitochondrial respiratory parameters, such as basal respiration, maximal respiration, and spare respiratory capacity (Figure 8g-l). The consistency between *in vivo* and *in vitro* results underscores that GK preserves mitochondrial integrity and function through coordinated activation of AMPK/Sirt1 signaling and suppression of pathological NF-κB activity, providing a mechanistic basis for its cardioprotective effects against DOX-induced injury.

DISCUSSION

As the final common pathway of cardiac diseases, HF exhibits a rising global incidence and mortality, highlighting the urgent need for research.[32] Current studies focus on elucidating mechanisms and developing innovative therapies, with particular attention to anticancer drug-induced myocardial injury. DOX-mediated cardiac damage exemplifies this challenge, frequently limiting its clinical use and adversely affecting patient prognosis.[33] Although existing preventive agents against DIC, such as dexrazoxane, mitigate oxidative damage through iron chelation, their clinical utility is constrained by modest efficacy and complications, such as bone marrow suppression.[34,35] These limitations underscore the critical need for improved therapeutic strategies. Natural compounds have recently gained attention as potential cardiovascular therapeutics

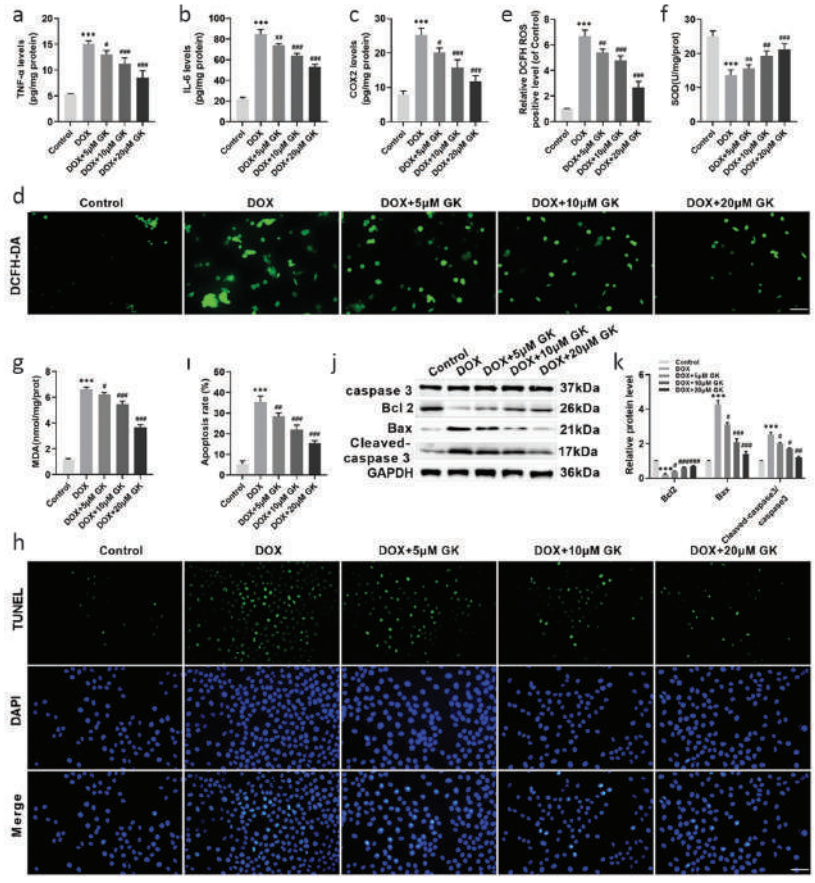

FIG. 6. GK attenuates DOX-induced cardiomyocyte inflammation, OS, and apoptosis. (a-c) Inflammatory mediators (TNF-α, IL-6, COX-2) in cardiomyocyte culture supernatants were quantified by ELISA to assess GK's anti-inflammatory effects against DOX stimulation. (d, e) ROS generation was measured fluorometrically using DCFH-DA oxidation. Scale bar 50 μm. (f, g) OS parameters (SOD activity, MDA content) were determined enzymatically to evaluate GK's antioxidant capacity. (h, i) Apoptotic incidence was quantified morphologically via TUNEL assay. Scale bar 50 μm. (j, k) Apoptotic pathway activation was examined by immunoblotting key regulators (Bax, Bcl-2, caspase-3 cleavage). n = 6. $^{***}p < 0.001$ vs. Control; ns $p > 0.05$, $^{\#}p < 0.05$, $^{\#\#}p < 0.01$, $^{\#\#\#}p < 0.001$ vs. DOX. DOX, doxorubicin; GK, ginkgetin; COX-2, cyclooxygenase-2; ROS, reactive oxygen species; ELISA, enzyme-linked immunosorbent assay; OS, oxidative stress; TNF-α, tumor necrosis factor-alpha; IL-6, interleukin-6; TUNEL, terminal deoxynucleotidyl transferase dUTP nick end labeling.

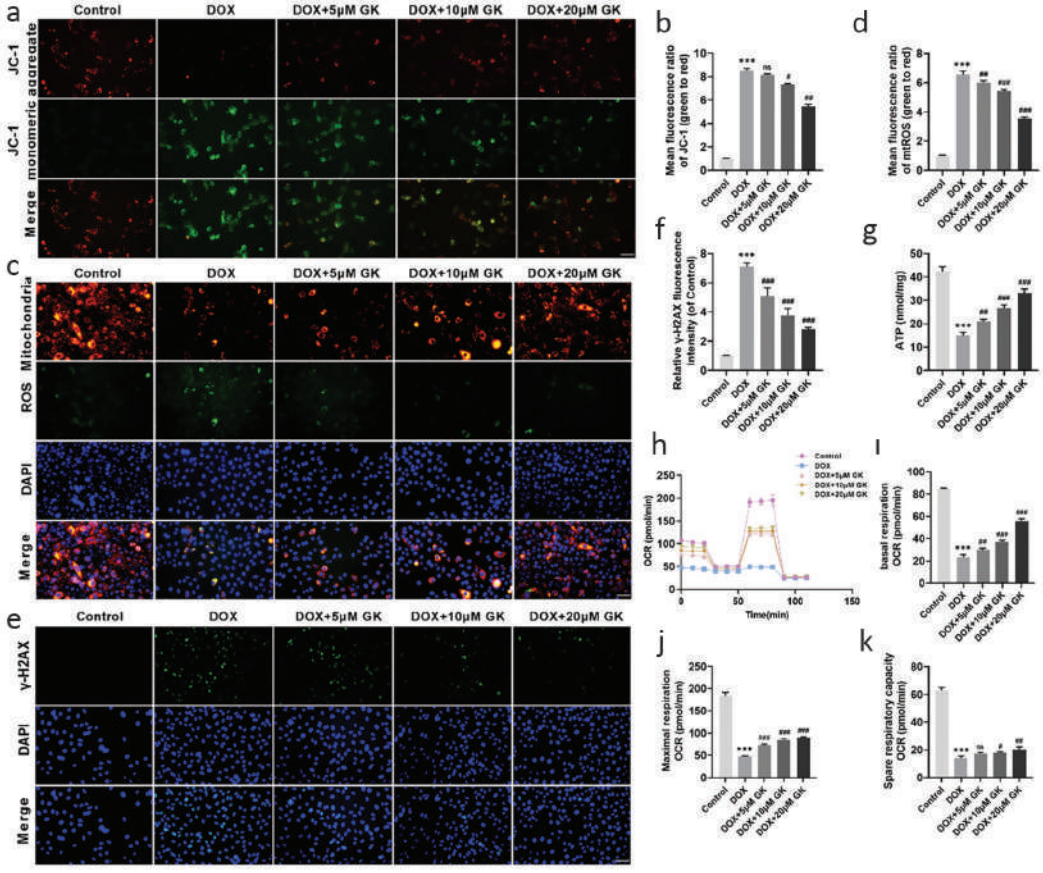

FIG. 7. GK ameliorates DOX-induced mitochondrial dysfunction in cardiomyocytes. (a, b) MMP alterations were evaluated using JC-1 fluorescent dye conversion. Scale bar 50 μm. (c, d) Dual-fluorescence imaging with MitoTracker-RFP (mitochondrial morphology, red) and ROS indicator (mitochondrial OS, green) enabled colocalization analysis of oxidative damage. Scale bar 50 μm. (e, f) γ-H2AX foci formation was quantified by immunofluorescence as a measure of DNA double-strand breaks. Scale bar 50 μm. (g) Cellular bioenergetics was assessed through ATP level quantification. (h-k) Mitochondrial respiratory parameters (basal/maximal respiration, spare capacity) were measured via Seahorse XFp metabolic flux analysis. n = 6. $^{***}p < 0.001$ vs. Control; ns $p > 0.05$, $^{\#}p < 0.05$, $^{\#\#}p < 0.01$, $^{\#\#\#}p < 0.001$ vs. DOX. DOX, doxorubicin; GK, ginkgetin; ROS, reactive oxygen species; OS, oxidative stress; MMP, mitochondrial membrane potential.

due to their multi-target activity, diverse molecular structures, and lower toxicity. For example, studies have demonstrated that ginkgolide K (GK) exhibits therapeutic effects in neurodegenerative and inflammatory diseases.[36,37] Despite these protective properties, GK's precise mechanisms against DOX-induced HF remain unclear. Using murine and cellular models of DOX cardiotoxicity, we systematically evaluated GK's cardioprotective effects. DOX-treated mice exhibited marked cardiac dysfunction, including decreased LVEF and fractional shortening (LVFS), as well as enlarged left ventricular internal diameters in systole and diastole (LVIDs/LVIDd). These changes reflect HF and align with observations in DIC models in rats.[38] LVEF and LVFS are key indicators of systolic function, and their reduction reflects impaired myocardial contractility.[39] Increased LVIDs and LVIDd indicate ventricular dilation and remodeling, markers of adverse cardiac remodeling.[40] GK treatment significantly improved these parameters, suggesting its ability to reverse DOX-induced systolic and diastolic dysfunction. Biochemical analysis further supported GK's protective role. LDH and CK-MB reflect cardiomyocyte membrane integrity,[41] cTnT is a myocardial-specific injury marker, and BNP is an established biomarker for HF diagnosis and prognosis.[42] GK treatment significantly reduced LDH, CK-MB, cTnT, and BNP levels, confirming its ability to preserve cardiomyocyte integrity. Histopathological examination demonstrated that GK alleviated DOX-induced myocardial damage, including cellular swelling, disordered architecture, collagen deposition, and myocardial hypertrophy. Cellular experiments corroborated these findings, showing GK's dose-dependent cytoprotective effects, evidenced by enhanced cell viability and reduced LDH release in DOX-challenged cardiomyocytes. In summary, GK exerts clear protective effects against DOX cardiotoxicity and shows promising potential as a candidate drug for HF therapy.

DIC is largely driven by myocardial OS. Studies show that DOX causes direct mitochondrial damage, impairing electron transport chain activity and increasing ROS production and release.[43,44] Excessive ROS attack cardiomyocyte lipids, proteins, and DNA, leading to membrane damage, enzyme inactivation, and gene mutations,

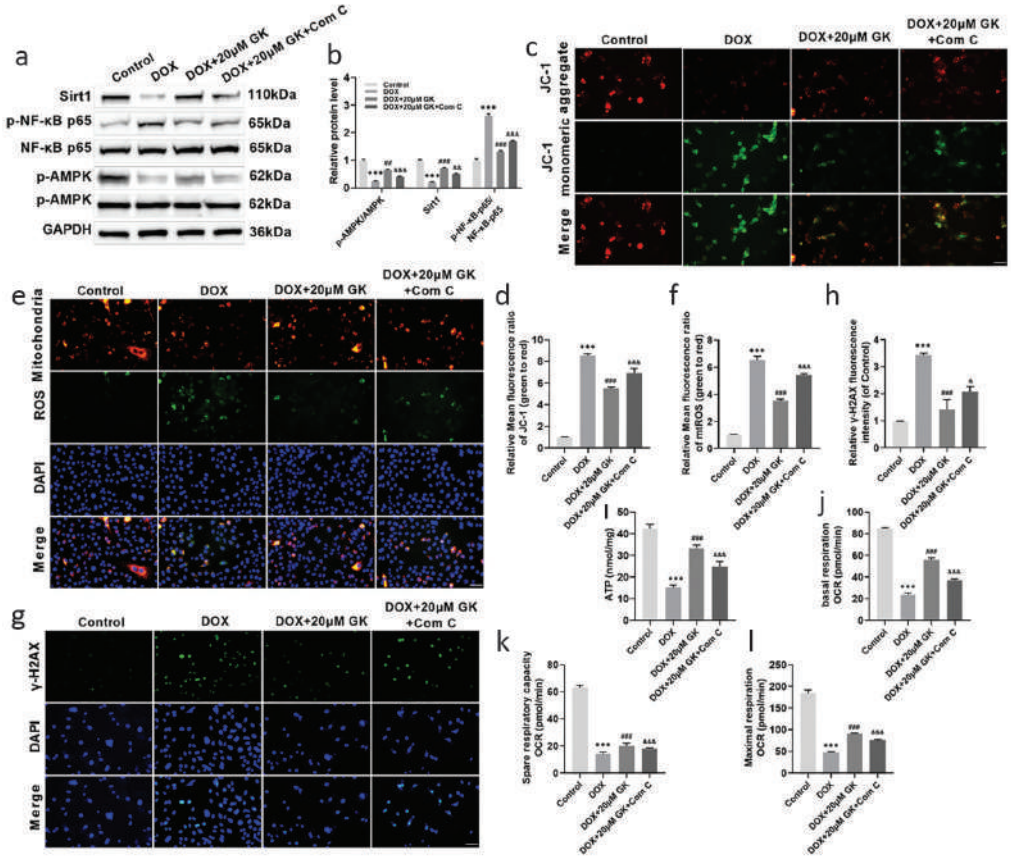

FIG. 8. GK alleviates DOX-induced cardiomyocyte injury by improving mitochondrial dysfunction through the AMPK/Sirt1/NF-κB signaling pathway. (a, b) To elucidate the cardioprotective mechanism of GK through the AMPK/Sirt1/NF-κB axis, H9c2 cells were divided into four experimental groups: Control, DOX, DOX + GK, and DOX + GK + Com C. Immunoblotting was performed to quantify the expression of AMPK/Sirt1/NF-κB pathway components, including total and phosphorylated forms of AMPK (p-AMPK) and NF-κB p65 (p-NF-κB p65), along with Sirt1. (c, d) MMP was evaluated using JC-1 fluorescence staining to assess mitochondrial functional integrity. Scale bar 50 μm. (e, f) Dual-fluorescence imaging with MitoTracker-RFP (mitochondrial morphology, red) and ROS indicator (mitochondrial OS, green) enabled colocalization analysis of oxidative damage. Scale bar 50 μm. (g, h) DNA damage was examined by immunofluorescence detection of γ-H2AX foci, followed by quantitative analysis of double-strand breaks. Scale bar 50 μm. (i) Cellular bioenergetic status was determined by measuring intracellular ATP levels. (j-l) Mitochondrial respiratory function was comprehensively assessed using the Seahorse XFp analyzer, with key parameters including basal respiration, maximal respiration, and spare respiratory capacity. n = 6. $^{***}p < 0.001$ vs. Control; $^{\#\#}p < 0.01$, $^{\#\#\#}p < 0.001$ vs. DOX, $^{\&}p < 0.05$, $^{\&\&}p < 0.01$, $^{\&\&\&}p < 0.001$ vs. DOX + GK. DOX, doxorubicin; GK, ginkgetin; NF-κB, nuclear factor-κB; OS, oxidative stress; MMP, mitochondrial membrane potential; AMPK, AMPK, adenosine monophosphate–activated protein kinase; ROS, reactive oxygen species.

ultimately causing cellular dysfunction or death.[45] In this study, GK significantly attenuated DOX-induced ROS, while enhancing SOD and GSH levels and reducing MDA, demonstrating strong antioxidant potential. Inflammation is another key contributor to DOX cardiotoxicity. DOX activates inflammatory cascades in cardiac cells and infiltrating immune cells, leading to excessive cytokine and chemokine release that aggravates myocardial injury and fibrosis.[46] Experimental data showed that GK markedly suppressed the elevated serum concentrations of inflammatory cytokines induced by DOX and modulated nitric oxide and COX-2 expression, confirming its anti-inflammatory capacity. The NF-κB pathway is a central regulator of inflammation. Under basal conditions, NF-κB is sequestered in the cytoplasm by IκB inhibitors.[47] Upon DOX exposure, IκB kinase is activated, leading to IκB phosphorylation and proteolytic degradation. This releases NF-κB dimers, which translocate to the nucleus and initiate transcription of multiple inflammatory genes by binding to κB regulatory sequences.[48] Western blot analysis in this study confirmed that GK inhibits DOX-induced NF-κB activation, which may underlie its anti-inflammatory effects. OS and inflammation interact closely, forming a positive feedback loop: ROS can activate NF-κB, and NF-κB activation can, in turn, increase ROS production.[49,50] This vicious cycle of "inflammation-OS" exacerbates myocardial injury. GK can simultaneously target these two pathological processes, suppressing DOX-induced myocardial inflammation and OS in mice, thereby effectively protecting the myocardium. These findings provide strong experimental evidence

supporting GK as a potential antioxidant and anti-inflammatory agent.

Mitochondrial impairment is a key pathological feature of HF, particularly in DOX-mediated cardiac injury.[51] Our study revealed that GK treatment effectively restored mitochondrial function in cardiac cells. In animal models, GK alleviated DOX-induced mitochondrial abnormalities through multiple mechanisms: preserving mitochondrial ultrastructure, minimizing DNA damage, increasing the expression of metabolic enzymes, and enhancing ATP production. These findings were corroborated by *in vitro* experiments, which showed that GK stabilizes MMP, attenuates OS, protects against DNA damage, and improves respiratory chain activity and energy production. The pathogenesis of HF involves critical contributions from AMPK, Sirt1, and NF-κB signaling pathways.[52-54] Our data indicate that GK upregulates AMPK and Sirt1 activity while downregulating NF-κB, collectively mitigating DOX-induced mitochondrial dysfunction. AMPK, a central cellular energy sensor, facilitates mitochondrial biogenesis and functional enhancement. When cellular energy stores are compromised, indicated by a decreased ATP/AMP ratio, AMPK is activated and phosphorylates downstream targets such as PGC-1α, thereby inducing mitochondrial gene transcription and improving mitochondrial quantity and function.[55] In this study, GK increased AMPK phosphorylation, suggesting that it promotes mitochondrial biogenesis via the AMPK-PGC-1α axis, counteracting DOX-mediated mitochondrial injury and enhancing myocardial energy metabolism. This aligns with previous reports showing that AMPK/Sirt1/PGC-1α activation ameliorates cardiac dysfunction by promoting mitochondrial biogenesis.[56] AMPK activation also enhances substrate metabolism by promoting glucose uptake and fatty acid oxidation,[8] providing essential precursors for mitochondrial function. To confirm the role of AMPK in GK's cardioprotective effects, we used siRNA-mediated knockdown of AMPK. In AMPK-deficient cells, GK's beneficial effects on Sirt1 expression and NF-κB p65 phosphorylation were significantly reversed (Supplementary Figure 1), demonstrating that AMPK is a key mediator of GK's actions and validating the specificity of the AMPK/Sirt1/NF-κB pathway. Sirt1, a NAD(+)-dependent deacetylase, plays a multifaceted role in mitochondrial regulation. It promotes mitochondrial biogenesis by deacetylating PGC-1α and also regulates mitochondrial dynamics (fusion and fission) and mitophagy.[57,58] Disrupted mitochondrial homeostasis and impaired mitophagy are hallmark features of DOX-mediated cardiac injury, resulting in accumulation of dysfunctional mitochondria.[59] Our results showed that GK upregulates Sirt1, indicating its potential to coordinate with AMPK signaling through Sirt1-dependent deacetylation to optimize mitochondrial function and facilitate the removal of damaged organelles.[60] The NF-κB pathway contributes to mitochondrial impairment and inflammatory activation. Upon activation, NF-κB triggers proinflammatory cytokine production, further aggravating mitochondrial dysfunction and establishing a self-perpetuating cycle of cellular injury.[61,62] GK inhibited DOX-induced NF-κB activation, thereby reducing inflammation and indirectly protecting mitochondria from inflammatory damage. Previous studies have shown that AMPK and Sirt1 negatively regulate NF-κB:[63] AMPK-mediated phosphorylation of IκBα prevents NF-κB nuclear translocation, while Sirt1-dependent deacetylation of p65 diminishes its DNA-binding capacity.[64,65] GK appears to coordinate this synergistic mechanism via AMPK/Sirt1 activation and NF-κB suppression, providing integrated protection against the multifaceted cardiac injury induced by DOX.

This study demonstrates that GK administration significantly attenuates DOX-induced cardiac injury, OS, inflammatory activation, apoptotic cell death, and mitochondrial dysfunction through the dual modulation of AMPK/Sirt1 activation and NF-κB suppression. These findings support GK's potential clinical application in preventing and managing chemotherapy-induced cardiac complications. An important limitation of this study is the relatively small sample size (n = 6 per group), which limits the precision of effect estimates and results in wide confidence intervals. For outcomes that did not reach statistical significance, the results should not be interpreted as indicating "no effect," as this may reflect insufficient statistical power, particularly for detecting small-to-medium effect sizes. Future studies with larger sample sizes are needed to validate these findings. Although animal models replicate certain aspects of human disease, interspecies differences in drug metabolism, signaling pathway regulation, and disease progression may exist. Therefore, these results require further validation in large animal models that more closely mimic human pathophysiology, followed by systematic preclinical and clinical studies to evaluate GK's therapeutic potential and safety in humans.

Ethics Committee Approval: Animal care and experimental procedures were conducted in accordance with regulations approved by the Aviation General Hospital Experimental Animal Ethics Committee (approval number: HK-X-2025-01, date: the date of the supplementary ethical annotation is: 13.01.2025).

Informed Consent: Not applicable.

Data Sharing Statement: The data that support the findings of this study are available from the corresponding author upon reasonable request.

Authorship Contributions: Concept- Y.P.; Design- C.W.; Funding- Y.Z.; Data Collection or Processing- W.L., Y.P.; Analysis and/or Interpretation- W.L.; Literature Review- X.R.; Writing- Y.W.; Critical Review- Y.W., Y.Z.

Conflict of Interest: The authors declare that they have no conflict of interest.

Funding: Based on the Aviation Industry Business Network platform, this paper explores the research on precise classification and grading of hypertension among aviation personnel and the intelligent diagnosis and treatment management model (No. YM2024ZD029).

Supplementary Figure: https://www.balkanmedicaljournal.org/img/files/2025-11-113.pdf

REFERENCES

1. Schwinger RHG. Pathophysiology of heart failure. *Cardiovasc Diagn Ther.* 2021;11:263-276. [CrossRef]
2. Lopaschuk GD, Karwi QG, Tian R, Wende AR, Abel ED. Cardiac energy metabolism in heart failure. *Circ Res.* 2021;128:1487-1513. [CrossRef]
3. Bozkurt B, Ahmad T, Alexander KM, et al.; Writing Committee Members. Heart failure epidemiology and outcomes statistics: a report of the Heart Failure Society of America. *J Card Fail.* 2023;29:1412-1451. [CrossRef]
4. Zhang S, Wu P, Liu J, Du Y, Yang Z. Roflumilast attenuates doxorubicin-induced cardiotoxicity by targeting inflammation and cellular senescence in cardiomyocytes mediated by SIRT1. *Drug Des Devel Ther.* 2021;15:87-97. [CrossRef]

5. Castiglione V, Aimo A, Vergaro G, et al. Biomarkers for the diagnosis and management of heart failure. *Heart Fail Rev*. 2022;27:625-643. [CrossRef]
6. Morciano G, Rimessi A, Patergnani S, et al. Calcium dysregulation in heart diseases: Targeting calcium channels to achieve a correct calcium homeostasis. *Pharmacol Res*. 2022;177:106119. [CrossRef]
7. Zhou L, Han Y, Yang Q, et al. Scutellarin attenuates doxorubicin-induced oxidative stress, DNA damage, mitochondrial dysfunction, apoptosis and autophagy in H9c2 cells, cardiac fibroblasts and HUVECs. *Toxicol In Vitro*. 2022;82:105366. [CrossRef]
8. Ng SM, Neubauer S, Rider OJ. Myocardial metabolism in heart failure. *Curr Heart Fail Rep*. 2023;20:63-75. [CrossRef]
9. Huang J, Li R, Wang C. The role of mitochondrial quality control in cardiac ischemia/reperfusion injury. *Oxid Med Cell Longev*. 2021;2021:5543452. [CrossRef]
10. Gallo G, Rubattu S, Volpe M. Mitochondrial dysfunction in heart failure: from pathophysiological mechanisms to therapeutic opportunities. *Int J Mol Sci*. 2024;25:2667. [CrossRef]
11. Yang HM. Mitochondrial dysfunction in cardiovascular diseases. *Int J Mol Sci*. 2025;26:1917. [CrossRef]
12. Han H, Li X, Guo Y, et al. Plant sterol ester of α-linolenic acid ameliorates high-fat diet-induced nonalcoholic fatty liver disease in mice: association with regulating mitochondrial dysfunction and oxidative stress via activating AMPK signaling. *Food Funct*. 2021;12:2171-2188. [CrossRef]
13. Hu L, Wang Z, Li H, et al. Icariin inhibits isoproterenol-induced cardiomyocyte hypertropic injury through activating autophagy via the AMPK/mTOR signaling pathway. *Biochem Biophys Res Commun*. 2022;593:65-72.[CrossRef]
14. Fan T, Zhu N, Li M, Wang Z, Lin X. CTRP6-mediated cardiac protection in heart failure via the AMPK/SIRT1/PGC-1α signalling pathway. *Exp Physiol*. 2024;109:2031-2045. [CrossRef]
15. Shan T, Li X, Xie W, et al. Rap1GAP exacerbates myocardial infarction by regulating the AMPK/SIRT1/NF-κB signaling pathway. *Cell Signal*. 2024;117:111080. [CrossRef]
16. Wang A J, Zhang J, Xiao M, et al. Molecular mechanisms of doxorubicin-induced cardiotoxicity: novel roles of sirtuin 1-mediated signaling pathways. *Cell Mol Life Sci*. 2021;78:3105-3125. [CrossRef]
17. Ibrahim KA, Abdelgaid HA, Eleyan M, Mohamed RA, Gamil NM. Resveratrol alleviates cardiac apoptosis following exposure to fenitrothion by modulating the sirtuin1/c-Jun N-terminal kinases/p53 pathway through pro-oxidant and inflammatory response improvements: In vivo and in silico studies. *Life Sciences*. 2022;290:120265. [CrossRef]
18. Luo Q, Zhang Q, Kong Y, Wang S, Wei Q. Heart failure, inflammation and exercise. *Int J Biol Sci*. 2025;21:3324-3350. [CrossRef]
19. Tatlı Çankaya İİ, Devkota HP, Zengin G, Šamec D. Neuroprotective potential of biflavone ginkgetin: a review. *Life (Basel)*. 2023;13:562. [CrossRef]
20. Jurčević Šangut I, Medvedec B, Šamec D. Establishment of in vitro callus culture of ginkgo (Ginkgo biloba L.) for studying the biosynthesis of 3', 8"-biflavones. PBE 2025 Budapest Programme and Book of Abstracts. 2025:181. [CrossRef]
21. Guo Y, Mao M, Li Q, Yu X, Zhou L. Extracts of Ginkgo flavonoids and ginkgolides improve cerebral ischaemia-reperfusion injury through the PI3K/Akt/Nrf2 signalling pathway and multicomponent in vivo processes. *Phytomedicine*. 2022;99:154028. [CrossRef]
22. Wei L, Jian P, Erjiong H, Qihan Z. Ginkgetin alleviates high glucose-evoked mesangial cell oxidative stress injury, inflammation, and extracellular matrix (ECM) deposition in an AMPK/mTOR-mediated autophagy axis. *Chem Biol Drug Des*. 2021;98:620-630. [CrossRef]
23. Li X, Luo W, Tang Y, et al. Semaglutide attenuates doxorubicin-induced cardiotoxicity by ameliorating BNIP3-Mediated mitochondrial dysfunction. *Redox Biol*. 2024;72:103129. [CrossRef]
24. Kosuru R, Kandula V, Rai U, Prakash S, Xia Z, Singh S. Pterostilbene decreases cardiac oxidative stress and inflammation via activation of AMPK/Nrf2/HO-1 pathway in fructose-fed diabetic rats. *Cardiovasc Drugs Ther*. 2018;32:147-163. [CrossRef]
25. Yu Y, Su FF, Xu C. Maximakinin reversed H_2O_2 induced oxidative damage in rat cardiac H9c2 cells through AMPK/Akt and AMPK/ERK1/2 signaling pathways. *Biomed Pharmacother*. 2024;174:116489. [CrossRef]
26. Wu X, Wang Z, Liang Z, et al. Pleiotropic role of CCR9/CCL25 signaling in adriamycin-induced cardiomyopathy. *J Adv Res*. 2025;75:707-722. [CrossRef]
27. Weng W, Yu X, Dong Y, et al. Artemether ameliorates adriamycin induced cardiac atrophy in mice. *Mol Med Rep*. 2023;28:153. doi: 10.3892/mmr.2023.13040.
28. Rong Z, Tu P, Xu P, et al. The mitochondrial response to DNA damage. *Front Cell Dev Biol*. 2021;9:669379. [CrossRef]
29. Trigo D, Avelar C, Fernandes M, Sá J, da Cruz E Silva O. Mitochondria, energy, and metabolism in neuronal health and disease. *FEBS Lett*. 2022;596:1095-1110. [CrossRef]
30. Li AL, Lian L, Chen XN, et al. The role of mitochondria in myocardial damage caused by energy metabolism disorders: From mechanisms to therapeutics. F*ree Radic Biol Med*. 2023;208:236-251. [CrossRef]
31. Wang Y, Wang Y, Yue G, Zhao Y. Energy metabolism disturbance in migraine: from a mitochondrial point of view. *Front Physiol*. 2023;14:1133528. [CrossRef]
32. Savarese G, Becher PM, Lund LH, et al. Global burden of heart failure: a comprehensive and updated review of epidemiology. *Cardiovasc Res*. 2023;118:3272-3287. Erratum in: *Cardiovasc Res*. 2023;119:1453. [CrossRef]
33. Sheibani M, Azizi Y, Shayan M, et al. Doxorubicin-induced cardiotoxicity: an overview on pre-clinical therapeutic approaches. *Cardiovasc Toxicol*. 2022;22:292-310. [CrossRef]
34. Arrigoni R, Jirillo E, Caiati C. Pathophysiology of doxorubicin-mediated cardiotoxicity. *Toxics*. 2025;13:277. [CrossRef]
35. Vitale R, Marzocco S, Popolo A. Role of oxidative stress and inflammation in doxorubicin-induced cardiotoxicity: a brief account. *Int J Mol Sci*. 2024;25:7477. [CrossRef]
36. Nowak A, Kojder K, Zielonka-Brzezicka J, et al. The Use of Ginkgo Biloba L. as a neuroprotective agent in the alzheimer's disease. *Front Pharmacol*. 2021;12:775034. [CrossRef]
37. Tao Z, Bai S, Wu G, et al. Therapeutic effect of ginkgetin on smoke-induced airway inflammation by down-regulating the c/EBPβ signaling pathway and CCL2 expression. *J Ethnopharmacol*. 2024;331:118284. [CrossRef]
38. Sun X, Zhou L, Han Y, et al. Scutellarin attenuates doxorubicin-induced cardiotoxicity by inhibiting myocardial fibrosis, apoptosis and autophagy in rats. *Chem Biodivers*. 2023;20:e202200450. [CrossRef]
39. Zhou C, Wu MZ, Liu Q, et al. Synergistic and attenuating effect of electroacupuncture on aconitine in improving heart failure and its calcium regulation mechanism. *Evid Based Complement Alternat Med*. 2022;2022:4940745. [CrossRef]
40. Yoon S, Gergs U, McMullen JR, Eom GH. Overexpression of heat shock protein 70 improves cardiac remodeling and survival in protein phosphatase 2a-expressing transgenic mice with chronic heart failure. *Cells*. 2021;10:3180. [CrossRef]
41. Liu Y, Niu Y, Zhang W, et al. Preparation of nanoparticles loaded with membrane-impermeable peptide AC3-I and its protective effect on myocardial ischemia and reperfusion. *Pharmaceutics*. 2024;16:416. [CrossRef]
42. Khan S, Rasool ST. Current use of cardiac biomarkers in various heart conditions. *Endocr Metab Immune Disord Drug Targets*. 2021;21:980-993. [CrossRef]
43. Wu BB, Leung KT, Poon EN. Mitochondrial-Targeted therapy for doxorubicin-induced cardiotoxicity. *Int J Mol Sci*. 2022;23:1912. [CrossRef]
44. Ling G, Wang X, Tan N, et al Mechanisms and drug intervention for doxorubicin-induced cardiotoxicity based on mitochondrial bioenergetics. *Oxid Med Cell Longev*. 2022;2022:7176282. [CrossRef]
45. Akhigbe R, Ajayi A. The impact of reactive oxygen species in the development of cardiometabolic disorders: a review. *Lipids Health Dis*. 2021;20:23. [CrossRef]
46. Bhagat A, Shrestha P, Kleinerman ES. The innate immune system in cardiovascular diseases and its role in doxorubicin-induced cardiotoxicity. *Int J Mol Sci*. 2022;23:14649. [CrossRef]
47. Mussbacher M, Derler M, Basílio J, Schmid JA. NF-κB in monocytes and macrophages - an inflammatory master regulator in multitalented immune cells. *Front Immunol*. 2023;14:1134661. [CrossRef]
48. Pakjoo M, Ahmadi SE, Zahedi M, et al. Interplay between proteasome inhibitors and NF-κB pathway in leukemia and lymphoma: a comprehensive review on challenges ahead of proteasome inhibitors. *Cell Commun Signal*. 2024;22:105. [CrossRef]
49. Yu Y, Zhu H, Shen M, et al. Sulfated cyclocarya paliurus polysaccharides exert immunomodulatory potential on macrophages via Toll-like receptor 4 mediated MAPK/NF-κB signaling pathways. *Food Science and Human Wellness*. 2024;13:115-123. [CrossRef]
50. Das S, Mukherjee T, Mohanty S, et al. Impact of NF-κB signaling and sirtuin-1 protein for targeted inflammatory intervention. *Curr Pharm Biotechnol*. 2025;26:1207-1220. [CrossRef]
51. Wu L, Wang L, Du Y, Zhang Y, Ren J. Mitochondrial quality control mechanisms as therapeutic targets in doxorubicin-induced cardiotoxicity. *Trends Pharmacol Sci*. 2023;44:34-49. [CrossRef]
52. Liu C, Guo X, Zhou Y, Wang H. AMPK Signalling pathway: a potential strategy for the treatment of heart failure with chinese medicine. *J Inflamm Res*. 2023;16:5451-5464. [CrossRef]

53. Li Z, Zhao H, Wang J. Metabolism and chronic inflammation: the links between chronic heart failure and comorbidities. *Front Cardiovasc Med*. 2021;8:650278. [CrossRef]
54. Yuan Q, Yang Z. Unraveling the therapeutic potential of ginsenoside compound Mc1 in Alzheimer's disease: Exploring the role of AMPK/SIRT1/NF-κB signaling pathway and mitochondrial function. *Adv Clin Exp Med*. 2024;33:1105-1114. [CrossRef]
55. Rodríguez C, Muñoz M, Contreras C, Prieto D. AMPK, metabolism, and vascular function. *FEBS J*. 2021;288:3746-3771. [CrossRef]
56. Chen M. Empagliflozin attenuates doxorubicin-induced cardiotoxicity by activating AMPK/SIRT-1/PGC-1α-mediated mitochondrial biogenesis. *Toxicol Res (Camb)*. 2023;12:216-223. [CrossRef]
57. Hou D, Liao H, Hao S, et al. Curcumin simultaneously improves mitochondrial dynamics and myocardial cell bioenergy after sepsis via the SIRT1-DRP1/PGC-1α pathway. *Heliyon*. 2024;10:e28501. [CrossRef]
58. Abu Shelbayeh O, Arroum T, Morris S, Busch KB. PGC-1α Is a master regulator of mitochondrial lifecycle and ROS stress response. *Antioxidants (Basel)*. 2023;12:1075. [CrossRef]
59. Chen R, Niu M, Hu X, He Y. Targeting mitochondrial dynamics proteins for the treatment of doxorubicin-induced cardiotoxicity. *Front Mol Biosci*. 2023;10:1241225. [CrossRef]
60. Yan W, Saqirile, Li K, Li K, Wang C. The role of N6-methyladenosine in mitochondrial dysfunction and pathology. *Int J Mol Sci*. 2025;26:3624. [CrossRef]
61. Singh S, Singh TG. Emerging perspectives on mitochondrial dysfunctioning and inflammation in epileptogenesis. *Inflamm Res*. 2021;70:1027-1042. [CrossRef]
62. Wu L, Chen Q, Dong B, et al. Resveratrol attenuated oxidative stress and inflammatory and mitochondrial dysfunction induced by acute ammonia exposure in gibel carp (Carassius gibelio). *Ecotoxicol Environ Saf*. 2023;251:114544. [CrossRef]
63. Lu Z, Wang H, Ishfaq M, et al. Quercetin and AMPK: a dynamic duo in alleviating MG-induced inflammation via the AMPK/SIRT1/NF-κB pathway. *Molecules*. 2023;28:7388. [CrossRef]
64. Tang TJ, Wang X, Wang L, et al. Liquiritin inhibits H_2O_2 -induced oxidative stress injury in H9c2 cells via the AMPK/SIRT1/NF-κB signaling pathway. *J Food Biochem*. 2022;46:e14351. [CrossRef]
65. Huang Q, Ren Y, Yuan P, et al. Targeting the AMPK/Nrf2 pathway: a novel therapeutic approach for acute lung injury. *J Inflamm Res*. 2024;17:4683-4700. [CrossRef]